



1 **Mineral physical protection and carbon stabilization in-situ evidence**
2 **revealed by nano scale 3-D tomography**

3 Yi-Tse Weng^{1,#}, Chun-Chieh Wang^{2,#}, Cheng-Cheng Chiang², Heng Tsai³, Yen-Fang
4 Song², Shiu-Tsuen Huang⁴, Biqing Liang^{1,*}

5 ¹National Cheng Kung University, Department of Earth Sciences, Tainan, Taiwan ROC

6 ²National Synchrotron Resource Research Center, Hsinchu, Taiwan ROC

7 ³National Changhua University of Education, Department of Geography, Changhua,
8 Taiwan ROC

9 ⁴National Taichung University of Education, Department of Science Education and
10 Application, Taichung, Taiwan ROC

11 #Equal Contribution

12 *Corresponding author: Biqing Liang
13 (liangglobalcarbon@gmail.com; liangbq@mail.ncku.edu.tw)

14

15 **Abstract**

16 An approach for nano scale 3-D tomography of organic carbon (OC) and
17 associated mineral nano particles was developed to illustrate their spatial distribution and
18 boundary interplay, using synchrotron-based transmission X-ray microscopy (TXM). The
19 proposed 3-D tomography technique was first applied to in-situ observation of a lab-made
20 consortium of black carbon (BC) and nano mineral (TiO₂, 15 nm), and its performance
21 was evaluated under dual-scan absorption contrast and phase contrast modes. Then this
22 novel tool was successfully applied to a natural OC-mineral consortium from high
23 mountain soil at a spatial resolution down to 60 nm, showing the fine structure and
24 boundary of OC, distribution of abundant minerals at nano size, and in-situ 3-D organo-
25 mineral association. The stabilization of aged natural OC was found attributed to the



1 physical protection of Fe-containing minerals (Fe oxyhydroxides including ferrihydrite,
2 goethite, and lepidocrocite) of nano size, and the strong organo-mineral complexation.
3 The sorption of OC (and cation) to Fe oxyhydroxides through organo-mineral multiple
4 complex bonds such as 'ligand exchange' could occupy and consume their respective
5 reactive surface sites, tune down their activity and enhance their respective stabilization.
6 The ubiquitousness and abundance of mineral nano particles, and their high
7 heterogeneity in natural environment could have been seriously underestimated by
8 traditional study approach. Our in-situ description of organo-mineral interplay at nano
9 scale provides direct evidence to substantiate the importance of mineral physical
10 protection for OC long term stabilization. Mineral physical protection for OC stabilization
11 may be more important than previous understanding. This high resolution 3-D
12 tomography tool is promising for new insight on the interior 3-D structure of micro-
13 aggregates, in-situ organo-mineral interplay, and the fate of mineral nano particles
14 including heavy metals in natural environment.

15

16 **Introduction**

17 Mineral association with organic carbon (OC) may be an important stabilization
18 mechanism for carbon long-term sequestration, yet little is known about their in-situ
19 interplay and extent of association on aggregation level either chemically or physically
20 (Baldock and Skjemstad, 2000; Cusack et al., 2012; Mikutta et al., 2006; Torn et al., 1997;
21 Vogel et al., 2014). Traditional fractionation methods based on size and external force for
22 dissecting the association strength between OC and minerals in soils are limited to bulk



1 sample. High resolution information and in-situ knowledge is required for interpretation of
2 fractionation results and modeling (Kaiser et al., 2002; Kleber et al., 2007; Sollins et al.,
3 2009). Nano scale two-dimensional isotopic mapping discovered that only a limited
4 amount of the clay-sized surfaces contributed to OC sequestration (Vogel et al., 2014).
5 Understanding OC interplay with minerals in the fine fraction warrants study in a three
6 dimensional way (Kinyangi et al., 2006; Lehmann et al., 2007; Lehmann et al., 2008;
7 Solomon et al., 2012). Detailed in-situ association information between OC and minerals
8 may lead to breakthrough on mineral physical protection mechanism for OC long term
9 stabilization. To overcome the limitations of commonly used electron microscopic
10 methods (such as only on the surface layer, and undesirable artifacts due to
11 pretreatments), non-destructive high-resolution X-ray 3-D tomographic technique will be
12 used for exploring the fine structure of OC and boundary interplay with mineral nano
13 particles.

14 High resolution Synchrotron-based TXM has been demonstrated as a powerful
15 tool for understanding the internal 3-D structure of particles down to nano meter scale,
16 due to its large penetration depth and superior spatial resolution (Kuo et al., 2011; Wang
17 et al., 2015). This technique was successfully applied to reveal the discrete three
18 dimensional micro-aggregation structure of clay (kaolinite) in natural aqueous
19 environment, and generated remarkable tomography that revealed precise inter-particle
20 structure (Zbik et al., 2008) as well. Clay particles with diameter below 500 nm were
21 clearly visible and their pseudohexagonal symmetry was recognized in details in a three
22 dimensional way.



1 The synchrotron-based TXM at the beamline BL01B1 of Taiwan Light Source
2 (TLS), which has been used in this study, provides two-dimensional imaging and three-
3 dimensional tomography at a spatial resolution of 30/60-nm with tunable energy (8-
4 11keV). It provides unprecedented opportunity for studying OC boundary interplays with
5 mineral particles at nano meter scale. Two image acquisition modes, absorption contrast
6 and phase contrast, can be used alternatively for recognizing OC and nano minerals.
7 Conventionally, X-ray images are taken in the absorption contrast mode, and the resulting
8 image contrast only depends on the difference of X-ray attenuation coefficient between
9 materials. This mode is especially useful for materials consisted of high atomic number
10 compositions. However, in organic materials, the difference of X-ray attenuation
11 coefficients between specimen and air is too small to distinguish each other. For this
12 reason, the structure of organic materials is often hard to be recognized due to low
13 contrast in absorption contrast images. Alternatively, phase contrast technique transfers
14 optical path length differences (optical phase) inside specimens into intensity contrast,
15 can be used for imaging low atomic number materials, which are poor to absorb X-rays.
16 It provides a unique opportunity to observe fine structures of organic specimens such as
17 OC. Little study has been done on OC and mineral nano particles using high-resolution
18 3-D X-ray tomography, though non-synchrotron-based 3-D X-ray microscopy was used
19 to observe occluded carbon in phytolith structure and kerogen in micrometer scale
20 (Alexandre et al., 2015; Bousige et al., 2016). We aim to develop a new dual-scan method
21 using phase contrast and absorption contrast modes of the TXM alternatively for the
22 observation of OC and mineral consortiums inside lab-made and natural samples in nano
23 meter scale. Lab-made OC in forms of black carbon (BC) will be examined in the artificial



1 consortium with added nano mineral (TiO₂) particles using synchrotron-based TXM for
2 the first time.

3 Black C/biochar has received increasing research interest globally due to its
4 importance in global carbon cycling, soil fertility improvement and environmental pollutant
5 remediation (Bond et al., 2013; Jeffery et al., 2015; Kuhlbusch, 1998; Lehmann et al.,
6 2007; Liang et al., 2006; Liang et al., 2008; Schmidt, 2004). On top of method
7 development for 3-D tomography at nano meter scale, this study provides in-situ
8 evidences on the minerals physical protection on natural OC, and to explore the C
9 stabilization mechanism in natural soil.

10

11 **Methodology**

12 **Sample preparation and background**

13 Black C was made in lab using leguminous plant (*Sesbania roxburghii*) of 80 days'
14 harvest, which was first oven-dried (65 °C) and charred inside a muffle furnace at 300 °C
15 in loosely sealed stainless containers (Chen et al., 2014b). This consortium of low
16 temperature BC and mineral nano particles was constructed by dry deposition of
17 commercial TiO₂ (15 nm) on lab-made BC (3 mm chunk), and then embedded in Gatan
18 G-1 epoxy. The block were cross sectioned to a thickness of 100 to 200 µm using a
19 microtome (Leica Reichert Ultracut E ultra-microtome) and subsequently hand-polished
20 to a thickness of 30 to 50 µm. Each section was transferred onto Kapton tape and
21 mounted on a stainless steel sample holder for TXM observation. Before TXM analysis,



1 gold nano particles (50-150 nm or 400-500 nm in diameter) were deployed on the section
2 surface for image registration before 3-D tomography reconstruction.

3 Thin section of natural OC and mineral consortium (NH) was prepared using
4 micron to millimeter size particulate sample from high mountain soil. Particulate organic
5 matter of mm-size with minerals embedded inside was taken from the lower dark layer at
6 depth of 72-93 cm in a Typic Humicryepts soil profile, located in Mt. Nanhua, Nantou
7 County, Taiwan (24°03'00", 121°17'02"). On top of this dark layer, iron stain was observed
8 within the depth of 63-72 cm in the profile. The soil has developed on top of sandstone
9 and slate, with some features of inceptisol and spodosol. The sampling elevation is 3092
10 m, the annual temperature is 7.57 °C, and the yearly rainfall is 2203.1 mm. The major
11 vegetation is arrow bamboo (*Yushania nittakayamensis*), with sporadic Hemlock (*Tsuga*
12 *chinensis*), fir (*Abies kawakamii*), and spruce (*Picea morrisonicola*).

13 The sequestration environment represents weak leaching and inactive chemical
14 weathering conditions. The age of soil organic C has been estimated to 3500 years B.P.

15

16 **Working conditions of TXM**

17 A superconducting wavelength shifter source provides a photon flux of 4×10^{11}
18 photons s^{-1} (0.1% bw) $^{-1}$ in the energy range of 5-20 KeV at the BL01B1 beamline. A
19 double crystal monochromator exploiting a pair of Ge (111) crystals selects X-rays within
20 the energy range of 8-11 KeV. The specimen is imaged using a Fresnel zone plate, which
21 is used as an objective lens for an image magnification of 44x by the first order diffraction



1 mode. Conjugated with a 20× downstream optical magnification, the TXM provides a total
2 magnification of 880× with a field of view of 15×15 μm². By acquiring a series of 2D
3 images with the sample rotated 1° stepwise, 3-D tomography datasets is later
4 reconstructed based on 151 sequential image frames that are captured with azimuth
5 angle rotating from -75° to +75°.

6

7 **Image acquisition for 3-D tomography**

8 Under the most frequently used absorption contrast mode, 2-D images are
9 recorded based on the projection of the different X-ray absorption coefficient integration
10 along the optical pathway through samples on a detector. The absorption mode is useful
11 for materials of high absorption coefficient, such as minerals or high atomic number
12 materials, but it is poor for the observation of low atomic number materials, such as
13 organic or polymer materials. In order to recognize the OC structure more accurately, 2-
14 D/3-D images for the same sample region are recorded using absorption contrast and
15 phase contrast modes, respectively.

16 In the phase contrast mode, the gold-made phase ring positioned at the back-focal
17 plane of the zone plate is used to retard or advance the phase of the non-diffractive light
18 by $\pi/2$, generating (Zernike's) phase contrast images recording at the detector. The light
19 diffracted by specimen is interfered with the retarded non-diffractive light, generating
20 phase contrast image. The intensity difference in a phase contrast image shows the



1 combination of optical phase difference and absorption difference through specimens.
2 This ability is especially important for the observation of OC which has a low X-ray
3 absorption coefficient.

4

5 **3-D reconstruction and analysis**

6 Three dimensional tomography reconstruction is performed using homemade
7 software, which is coded based on iterative image registration (Faproma) (Wang et al.
8 2017) and filtered back projection (FBP) reconstruction algorithms. Firstly, a serial of
9 single TXM image captured from -75° to $+75^{\circ}$ at rotational increments of 1° is loaded to
10 do image registration automatically using Faproma algorithm. Finally, the reconstruction
11 is processed using FBP algorithm. The reconstructed dataset is exported in cross-
12 sections, and later used for 3-D visualization using *Amira*. The intensity contrast of
13 reconstructed datasets is inversed for better visualization; Compositions with higher
14 absorption coefficients are shown in higher intensity and with low absorption coefficients
15 are shown in lower intensity. The exported cross-section of 3-D tomography
16 (reconstructed datasets) shows the real distribution details and boundary interplay of OC
17 and mineral particles. The final 3-D tomographic structures for visualization and
18 illustration are generated using *Amira* 3-D software for image post-process and
19 computation (Fig. S1).

20

21 **Elemental mapping by SEM-EDS**



1 For correlated spatial distribution of selected elements (C, O, Fe, Al) in natural OC
2 particles from high mountain soil, a low-vacuum scanning electron microscope (JEOL W-
3 LVSEM, JSM-6360LV) equipped with an energy dispersive X-ray spectrometer (Oxford
4 EDS) and a cathodoluminescence (CL) image detector (Gatan mini-CL) was used for
5 elemental mapping, at an accelerating voltage of 15 KeV.

6

7 **X-ray Diffraction for Mineralogy**

8 To analyze the forms of minerals associated with natural OC, particulate OC (with
9 minerals on surface and embedded inside) was grounded and injected into capillary tubes
10 (Special Glass 10, Hampton Research, CA) for synchrotron high resolution X-ray
11 diffraction analysis at 09A beamline at Taiwan Photon Source (TPS), which is equipped
12 with a set of high-resolution monochromator (HRM). The wavelength is 0.8266 Å at the
13 energy of 15 KeV. The XRD spectra were recorded under room temperature for 240s
14 accumulation time and specific X-ray diffraction peaks and patterns were assigned ICDD
15 using PDF-2/4 program.

16

17 **Carbon functionality and interfacial mineral forms using SR-FTIR**

18 For FTIR analysis, mineral-bearing OC (NH) particles were grounded, dried (60 °C
19 overnight), and mixed with potassium bromide (KBr) at a ratio of 1:100, and molded into
20 disks using a hydraulic press. During the pressing process, a vacuum pump was used for
21 evacuating air and water. The samples were measured using Infrared



1 Microspectroscopy (IMS) at the BL14A1 beamline of the National Synchrotron Radiation
2 Research Center (NSRRC), Taiwan. The FTIR spectra were collected up to 1024 scans
3 in the mid-infrared range of 4000-400 cm^{-1} with a spectral resolution of 4 cm^{-1} , using a
4 FTIR spectrometer (Nicolet 6700, Thermo Fisher Scientific, Madison, WI, USA) with a
5 self-equipped light source. The automatic atmospheric suppression function in OMNIC
6 (OMNIC 9.2, 2012; Thermo Fisher Scientific Inc., Waltham, MA, USA) for bulk sample
7 analysis was activated for data analysis, to eliminate the rovibration absorptions of CO_2
8 and water vapor in ambient air.

9

10 **Results and Discussions**

11 **Distinguish the fine structure of BC and boundary interplay with mineral nano** 12 **particles**

13 High resolution 2-D X-ray photographs were captured for the identical regions in
14 lab-made BC and nano mineral consortium using dual-scan absorption contrast and
15 phase contrast modes (Fig. 1, a, e). The cross-section views exported from the
16 reconstructed 3-D datasets reveal subtle details of BC and mineral nano particles, and
17 clearly outline the fine boundary of BC and the distribution of TiO_2 nano particles (Fig. 1).
18 The shape, size, and distribution of mineral nano particles can be identified accurately
19 using absorption contrast mode due to their high X-ray absorptivity (Fig.1, b, c and d). In
20 comparison, the BC structure and contour of its boundary can be revealed much more
21 clearly using phase contrast mode (Fig.1, f, g and h). However, the bright halo artifacts in
22 phase-contrast image enhance the intensity of margin texture for nano minerals, and may



1 lead to overestimation of their volume (Fig. 1, e, f, g and h). Use of dual-scan mode allows
2 cross-checking of details and validation.

3 Cross-section views of the reconstructed 3-D tomography share consistent and
4 comparable features of BC and nano minerals in multi-angles (Fig. 2). According to the
5 display of different slicing planes (XY, XZ, YZ), it can be recognized that TiO₂ nano
6 particles deposit inside BC only sporadically contact with BC boundary (Fig. 2, b, e, c,
7 and f) due to the treatment of dry deposition. The nano scale gap between BC and nano
8 minerals has been clearly observed in absorption and phase-contrast images (Fig. 2, b,
9 e, c, and f). It is feasible to calculate the interplay surface and mineral volume
10 quantitatively by examining each cross-section views in a selected region. Our approach
11 is a success in thorough exploration of OC and minerals 3-D distribution, and verification
12 of their real in-situ spatial correlation under nano scale resolution.

13

14 **3-D tomography for illustrating in-situ distribution of BC and mineral nano particles**

15 3-D tomography for visualization has been computed and generated to illustrate
16 the spatial correlation between BC and minerals based on post-process of reconstructed
17 3-D datasets. Unprecedented details of 3-D in-situ distribution of BC and mineral nano
18 particles are revealed in computed 3-D tomography (Fig. 3; Fig. SMOV1, 2). Results from
19 absorption mode and phase contrast mode are consistent and comparable. The fine
20 boundary feature of BC is contoured to a more completeness in the phase contrast mode.
21 The OC was rendered by transparent mode and high absorptivity materials (such as



1 minerals and gold particles) were rendered by solid mode with various colors. All
2 renderings are combined to visualize their interaction. The illustration of 3-D computed
3 tomography allows randomly tilted and set angles for image and animated video exports,
4 thus any region of interest inside a specimen may be explored thoroughly.

5 The lab-made consortium was successfully tested by this dual-scan methodology
6 using both absorption contrast and phase-contrast acquisition modes (Figs. 1, 2, 3). Low
7 temperature BC, which is more similar to natural OC (especially recalcitrant OC) than that
8 made at high temperature, was especially made to test its applicability under absorption
9 contrast mode. Results show that the fine structure and boundary of low temperature BC
10 can be clearly observed under absorption contrast mode. Thus for environmental OC
11 samples, the use of absorption contrast mode is probably sufficient for capturing organo-
12 mineral features.

13 Different from field samples, the minerals observed within the lab-made consortium
14 often distribute in clusters and are only sparsely in association with BC surface. The
15 preservation of plant-like structures in BC could play a role for carbon stabilization in
16 natural environment, as their porosity and reactive surface provide large areas and sites
17 for mineral coating, which may contribute to their long residence and physical endurance
18 (Eusterhues et al., 2008; Rasmussen et al., 2005; Rawal et al., 2016).

19

20 **Interplay of OC and minerals and C stabilization in high mountain soil**



1 Nano scale 3-D tomography provides new insight for the mineral physical
2 protection mechanism of OC in soil. Natural OC exhibited strong organo-mineral
3 association on its surface at nano scale in high mountain soil (Fig. 4; Fig. SMOV3).
4 Abundant short-range order minerals in forms of subhedral particle or anhedral nano-
5 aggregate have direct contact with the boundary of OC and develop coating on the
6 tracheid surface (Fig. 4 b and c) (Mikutta et al., 2006). Mineral aggregation by poorly
7 crystalline nano particles renders natural sub-micron porosity, which may contribute to
8 elevated sorption capacity in soil (Rawal et al., 2016). The densely-packed mineral texture
9 suggested significant physical protection on OC surface (Kaiser and Guggenberger,
10 2007). The sorbed minerals not only can form physical protection, but also could shield
11 OC from chemical weathering (Mikutta et al., 2006).

12 The nature of associated minerals was confirmed to be mainly Fe oxyhydroxides,
13 specifically ferrihydrite (ICDD 01-073-8408), goethite (ICDD 01-073-6522), lepidocrocite
14 (ICDD 00-044-1415), and quartz (ICDD 00-033-1161) (Fig. 5; Table S1), analyzed using
15 high resolution synchrotron-based XRD. Quartz may be at most a minor component on
16 OC surface, considering their chemistry and particle size. Yet siliceous mineral surfaces
17 may become coated with a veneer of hydrous Al- and Fe- oxides, which could confer net
18 positive charge and promote their reactivity in tropical environments (Chen et al., 2014a;
19 Sposito, 1989).

20 Considering their high surface area and reactivity, the abundant nano scale Fe
21 oxyhydroxides could play a significant role for OC long-term stabilization through
22 chemical bonding and physical shielding (Eusterhues et al., 2005; Kaiser et al., 2002;



1 Kiem and Kogel-Knabner, 2002; Mikutta et al., 2006), as well as cation sorption in soil,
2 and contribute to longevity of OC in high mountain soil. According to elemental mapping
3 results, aluminosilicates may also be present, however, their portion and crystalline level
4 should be low due to their minimal signal in the XRD spectra (Figs. 5, 6). The FTIR
5 analyses reveal the chemistry of organo-mineral association (Fig. 7; Table S2). The aged
6 OC is highly aromatic when at the same time highly reactive, as broad bands centered at
7 1596 cm^{-1} and 1706 cm^{-1} for aromatic C=C stretching and $\nu\text{ C=O}$ in carboxyl are
8 observed, pointing to likely origin of pyrogenic C (Özçimen and Ersoy-Meriçboyu, 2010;
9 Sharma et al., 2004). Both aromatic and carboxyl C functional groups normally have high
10 affinity with Fe (III) (Mikutta et al., 2007; Zhao et al., 2016). The broad bands point to
11 possible significant degree of association between OC and minerals (Chen et al., 2016;
12 Gu et al., 1994; Kaiser and Guggenberger, 2007). The sorption of OC to Fe oxyhydroxides
13 through organo-mineral multiple complex bonds such as 'ligand exchange' could occupy
14 and consume the reactive surface sites on OC and Fe oxyhydroxides, tune down their
15 activity and enhance their respective stabilization (Chorover and Amistadi, 2001; Cornell
16 and Schwertmann, 2006; Hall et al., 2016; Kaiser and Guggenberger, 2007; Mikutta et
17 al., 2007). The discovery of short-range-order mineral ferrihydrite in air-dried OC particles
18 and later ground samples indirectly validates its stabilization due to organo-mineral
19 interplay. As a metastable mineral, ferrihydrite is hard to estimate accurately in dry soil
20 samples due to its transient nature and the limitation of traditional extraction and
21 spectroscopic methods (Cornell and Schwertmann, 2006). The specific mineral forms in
22 direct contact with OC on surface at nano scale warrants future study (Fig. SMOV3). In-



1 situ mineral mapping of different Fe oxyhydroxide on OC surface will provide mechanistic
2 evidence on OC stabilization. Mineral physical protection on OC may represent the end
3 stage of carbon stabilization, especially in a weak leaching and weathering environment.

4 Our in-situ description of organo-mineral interplay at nano scale provides direct
5 evidence on the important role of mineral physical protection for OC long term stabilization.
6 High amounts of ferrihydrite and other Fe oxyhydroxides were also found associated with
7 lignin-like OC in soil under an aquic moisture regime (Eusterhues et al., 2011). The
8 abundance of mineral nano particles, and their high heterogeneity and short-range-order
9 nature could be common in humid environment, however, they could have been seriously
10 underestimated by traditional analysis methods (Mikutta et al., 2005). Mineral physical
11 protection for OC stabilization may be more important than previous understanding.

12 In summary, a high resolution 3-D tomography tool is required for exploring the in-
13 situ interplay of OC and nano minerals in natural environment. Nano scale 3-D
14 tomography provides direct evidence and new insight for the mineral physical protection
15 mechanism of OC in soil. This high resolution 3-D tomography approach is a promising
16 technique for probing the multi interfacial features between OC and minerals in lab and
17 field samples, and may provide new perspective on the fate of nano particles including
18 heavy metals in natural environments.

19

20

21 **Figure Captions**



1 **Figure 1.** The 2-D X-ray images for the same region of BC and mineral nano particle
2 consortium obtained using absorption contrast mode **(a)** and phase contrast mode **(e)**.
3 Cross-section views of the reconstructed 3-D tomography under each mode at different
4 depths relative to the position of gold nano particle along Z-axis as a reference. **(b)** and
5 **(f)** are sections extracted at the position of the gold particle. **(c)** and **(g)** are sections
6 extracted at 800 nm above the gold particle. **(d)** and **(h)** are sections extracted at 800 nm
7 below the gold particle. The scale bar is 5 μm .

8 **Figure 2.** Three-directional orthogonal sections of lab-made BC and mineral nano particle
9 consortium. The upper row sections are extracted from absorption contrast tomography
10 **(a, b, c)**, and the lower row sections are extracted from phase contrast tomography **(d, e,**
11 **f)**, specifically **(a)** and **(d)** are for XY plane, **(b)** and **(e)** are for YZ plane, and **(c)** and **(f)**
12 are for XZ plane. The scale bar is 5 μm .

13 **Figure 3.** 3-D tomography illustration of lab-made BC and mineral nano particle
14 consortium observed at -45° **(a, d)**, 0° **(b, e)**, and $+45^\circ$ **(c, f)** azimuthal viewing angles
15 under absorption contrast **(a, b, c)** and phase contrast mode **(d, e, f)**. The scale bar is 5
16 μm .

17 **Figure 4.** Three-directional orthogonal sections of high mountain mineral-bearing OC
18 from absorption contrast tomography **(a** for XY plane, **b** for XZ plane, and **c** for YZ plane). .
19 The scale bar is 5 μm . Minerals mainly present two types of textures, subhedral particles
20 and anhedral nano-aggregates. The lower row images highlight the free surface of
21 specimen (red line in **d**), the boundary of OC (green dotted-line in **e**), and the subhedral
22 mineral particles (pink arrow in **e** and **f**)



1 **Figure 5.** The X-ray diffraction pattern of minerals within OC particles from high mountain
2 soil. Highly reactive Fe oxyhydroxides are identified and denoted with lines of different
3 colors: ferrihydrite (ICDD 01-073-8408, orange), goethite (ICDD 01-073-6522, blue), and
4 lepidocrocite (ICDD 00-044-1415, green). Q stands for Quartz (ICDD 00-033-1161).
5 Details are included in Table S1.

6 **Figure 6.** Elementary mapping by SEM-EDS for mineral-bearing OC from high mountain
7 soil. Left: SEM backscattering image (The bright spots inside are gold nano particles for
8 coating). Right: Elemental mapping of C, O, Fe and Al. Scale bars are 20 μm .

9 **Figure 7.** The FTIR spectra for the chemistry of organo-mineral association. The aged
10 OC is highly aromatic (1596 and 1386 cm^{-1}), and highly reactive with obvious carboxyl
11 functional group (1706 cm^{-1}). The broad bands point to possible significant degree of
12 association between OC and minerals. Some minor bands near 1274 , 1062 , 1024 , and
13 989 cm^{-1} indicate the lignin-derived nature of OC. Those bands near 476 , 534 , 798 , 910
14 and 1025 cm^{-1} have similar characteristics of soil inorganic/mineral matrix. More details
15 are included in Table S2.

16

17

18 **Acknowledgement**

19 We thank Dr. Chung-Ho Wang for kind support, the technical support from Ms. Hsueh-
20 Chi Wang (TXM, TLS-BL01B01); Dr. Yao-Chang Lee and Ms. Pei-Yu Huang (FTIR, TLS-
21 BL14A1); and Dr. Hwo-Shuenn Sheu and Dr. Yu-Chun Chuang (XRD, TPS-09A1) at the



1 end-stations of NSRRC (Taiwan), the help for SEM-EDS analysis from Dr. Yoshiyuki
2 Iizuka (Academia Sinica), the SC specimen from Dr. Chih-Hsin Cheng (National Taiwan
3 University), the TiO₂ nano particles from Dr. Yen-Hua Chen (NCKU, the department of
4 Earth Sciences), and Dr. Chia-Chuan Liu, the former and current members of the NCKU
5 Global Change Geobiology Carbon Laboratory for help and support.

6

7

8 **Funding Sources**

9 BQ Liang and CC Wang acknowledged the funding support from Taiwan Ministry of
10 Science and Technology (MOST 102-2116-M-006-018-MY2, MOST 105-2116-M-006-
11 010-, and MOST 105-2112-M-213-001).

12

13

14 **References**

15 Alexandre, A., Basile-Doelsch, I., Delhaye, T., Borshneck, D., Mazur, J. C., Reyerson,
16 P., and Santos, G. M.: New highlights of phytolith structure and occluded carbon
17 location: 3-D X-ray microscopy and NanoSIMS results, *Biogeosciences*, 12, 863-
18 873, 2015.

19 Baldock, J. A. and Skjemstad, J. O.: Role of the soil matrix and minerals in protecting
20 natural organic materials against biological attack, *Org. Geochem.*, 31, 697-710,
21 2000.

22 Bond, T. C., Doherty, S. J., Fahey, D. W., Forster, P. M., Berntsen, T., DeAngelo, B. J.,
23 Flanner, M. G., Ghan, S., Karcher, B., Koch, D., Kinne, S., Kondo, Y., Quinn, P. K.,
24 Sarofim, M. C., Schultz, M. G., Schulz, M., Venkataraman, C., Zhang, H., Zhang,
25 S., Bellouin, N., Guttikunda, S. K., Hopke, P. K., Jacobson, M. Z., Kaiser, J. W.,



- 1 Klimont, Z., Lohmann, U., Schwarz, J. P., Shindell, D., Storelvmo, T., Warren, S.
2 G., and Zender, C. S.: Bounding the role of black carbon in the climate system: A
3 scientific assessment, *J. Geophys. Res-Atmos.*, 118, 5380-5552, 2013.
- 4 Bousige, C., Ghimbeu, C. M., Vix-Guterl, C., Pomerantz, A. E., Suleimenova, A.,
5 Vaughan, G., Garbarino, G., Feygensohn, M., Wildgruber, C., Ulm, F.-J., Pellenq, R.
6 J. M., and Coasne, B.: Realistic molecular model of kerogen's nanostructure,
7 *Nature Materials*, 15, 576, 2016.
- 8 Chen, C., Dynes, J. J., Wang, J., Karunakaran, C., and Sparks, D. L.: Soft X-ray
9 Spectromicroscopy Study of Mineral-Organic Matter Associations in Pasture Soil
10 Clay Fractions, *Environ. Sci. Technol.*, 48, 6678-6686, 2014a.
- 11 Chen, C. P., Cheng, C. H., Huang, Y. H., Chen, C. T., Lai, C. M., Menyailo, O. V., Fan,
12 L. J., and Yang, Y. W.: Converting leguminous green manure into biochar: changes
13 in chemical composition and C and N mineralization, *Geoderma*, 232, 581-588,
14 2014b.
- 15 Chen, K.-Y., Chen, T.-Y., Chan, Y.-T., Cheng, C.-Y., Tzou, Y.-M., Liu, Y.-T., and Teah,
16 H.-Y.: Stabilization of Natural Organic Matter by Short-Range-Order Iron
17 Hydroxides, *Environ. Sci. Technol.*, 50, 12612-12620, 2016.
- 18 Chorover, J. and Amistadi, M. K.: Reaction of forest floor organic matter at goethite,
19 birnessite and smectite surfaces, *Geochim. Cosmochim. Acta*, 65, 95-109, 2001.
- 20 Cornell, R. M. and Schwertmann, U.: *The Iron Oxides: Structure, Properties, Reactions,*
21 *Occurrences and Uses*, Wiley, 2006.
- 22 Cusack, D. F., Chadwick, O. A., Hockaday, W. C., and Vitousek, P. M.: Mineralogical
23 controls on soil black carbon preservation, *Global Biogeochem. Cy.*, 26, 2019,
24 2012.
- 25 Eusterhues, K., Rennert, T., Knicker, H., Kögel-Knabner, I., Totsche, K. U., and
26 Schwertmann, U.: Fractionation of Organic Matter Due to Reaction with
27 Ferrihydrite: Coprecipitation versus Adsorption, *Environ. Sci. Technol.*, 45, 527-
28 533, 2011.



- 1 Eusterhues, K., Rumpel, C., and Kögel-Knabner, I.: Organo-mineral associations in
2 sandy acid forest soils: importance of specific surface area, iron oxides and
3 micropores, *Eur. J. Soil Sci.*, 56, 753-763, 2005.
- 4 Eusterhues, K., Wagner, F. E., Häusler, W., Hanzlik, M., Knicker, H., Totsche, K. U.,
5 Kögel-Knabner, I., and Schwertmann, U.: Characterization of Ferrihydrite-Soil
6 Organic Matter Coprecipitates by X-ray Diffraction and Mössbauer Spectroscopy,
7 *Environ. Sci. Technol.*, 42, 7891-7897, 2008.
- 8 Gu, B. H., Schmitt, J., Chen, Z. H., Liang, L. Y., and Mccarthy, J. F.: Adsorption and
9 Desorption of Natural Organic-Matter on Iron-Oxide - Mechanisms and Models,
10 *Environ. Sci. Technol.*, 28, 38-46, 1994.
- 11 Hall, S. J., Silver, W. L., Timokhin, V. I., and Hammel, K. E.: Iron addition to soil
12 specifically stabilized lignin, *Soil Biol. Biochem.*, 98, 95-98, 2016.
- 13 Jeffery, S., Bezemer, T. M., Cornelissen, G., Kuyper, T. W., Lehmann, J., Mommer, L.,
14 Sohi, S. P., van de Voorde, T. F. J., Wardle, D. A., and van Groenigen, J. W.: The
15 way forward in biochar research: targeting trade-offs between the potential wins,
16 *GCB. Bioenergy*, 7, 1-13, 2015.
- 17 Kaiser, K., Eusterhues, K., Rumpel, C., Guggenberger, G., and Kogel-Knabner, I.:
18 Stabilization of organic matter by soil minerals - investigations of density and
19 particle-size fractions from two acid forest soils, *J. Plant Nutr. Soil Sci.*, 165, 451-
20 459, 2002.
- 21 Kaiser, K. and Guggenberger, G.: Sorptive stabilization of organic matter by
22 microporous goethite: sorption into small pores vs. surface complexation, *Eur. J.*
23 *Soil Sci.*, 58, 45-59, 2007.
- 24 Kiem, R. and Kogel-Knabner, I.: Refractory organic carbon in particle-size fractions of
25 arable soils II: organic carbon in relation to mineral surface area and iron oxides in
26 fractions < 6 μ m, *Org. Geochem.*, 33, 1699-1713, 2002.
- 27 Kinyangi, J., Solomon, D., Liang, B., Lerotic, M., Wirick, S., and Lehmann, J.:
28 Nanoscale Biogeocomplexity of the Organomineral Assemblage in Soil, *Soil Sci.*
29 *Soc. Am. J.*, 70, 1708-1718, 2006.



- 1 Kleber, M., Sollins, P., and Sutton, R.: A conceptual model of organo-mineral
2 interactions in soils: self-assembly of organic molecular fragments into zonal
3 structures on mineral surfaces, *Biogeochemistry*, 85, 9-24, 2007.
- 4 Kuhlbusch, T. A. J.: Black carbon and the carbon cycle, *Science*, 280, 1903-1904, 1998.
- 5 Kuo, C.-H., Chu, Y.-T., Song, Y.-F., and Huang, M. H.: Cu₂O Nanocrystal-Templated
6 Growth of Cu₂S Nanocages with Encapsulated Au Nanoparticles and In-Situ
7 Transmission X-ray Microscopy Study, *Adv. Funct. Mater.*, 21, 792-797, 2011.
- 8 Lehmann, J., Kinyangi, J., and Solomon, D.: Organic matter stabilization in soil
9 microaggregates: implications from spatial heterogeneity of organic carbon
10 contents and carbon forms, *Biogeochemistry*, 85, 45-57, 2007.
- 11 Lehmann, J., Solomon, D., Kinyangi, J., Dathe, L., Wirick, S., and Jacobsen, C.: Spatial
12 complexity of soil organic matter forms at nanometre scales, *Nat. Geosci.*, 1, 238-
13 242, 2008.
- 14 Liang, B., Lehmann, J., Solomon, D., Kinyangi, J., Grossman, J., O'Neill, B., Skjemstad,
15 J. O., Thies, J., Luizao, F. J., Petersen, J., and Neves, E. G.: Black Carbon
16 increases cation exchange capacity in soils, *Soil Sci. Soc. Am. J.*, 70, 1719-1730,
17 2006.
- 18 Liang, B., Lehmann, J., Solomon, D., Sohi, S., Thies, J. E., Skjemstad, J. O., Luizão, F.
19 J., Engelhard, M. H., Neves, E. G., and Wirick, S.: Stability of biomass-derived
20 black carbon in soils, *Geochim. Cosmochim. Acta*, 72, 6069-6078, 2008.
- 21 Mikutta, R., Kleber, M., and Jahn, R.: Poorly crystalline minerals protect organic carbon
22 in clay subfractions from acid subsoil horizons, *Geoderma*, 128, 106-115, 2005.
- 23 Mikutta, R., Kleber, M., Torn, M. S., and Jahn, R.: Stabilization of Soil Organic Matter:
24 Association with Minerals or Chemical Recalcitrance?, *Biogeochemistry*, 77, 25-56,
25 2006.
- 26 Mikutta, R., Mikutta, C., Kalbitz, K., Scheel, T., Kaiser, K., and Jahn, R.: Biodegradation
27 of forest floor organic matter bound to minerals via different binding mechanisms,
28 *Geochim. Cosmochim. Acta*, 71, 2569-2590, 2007.

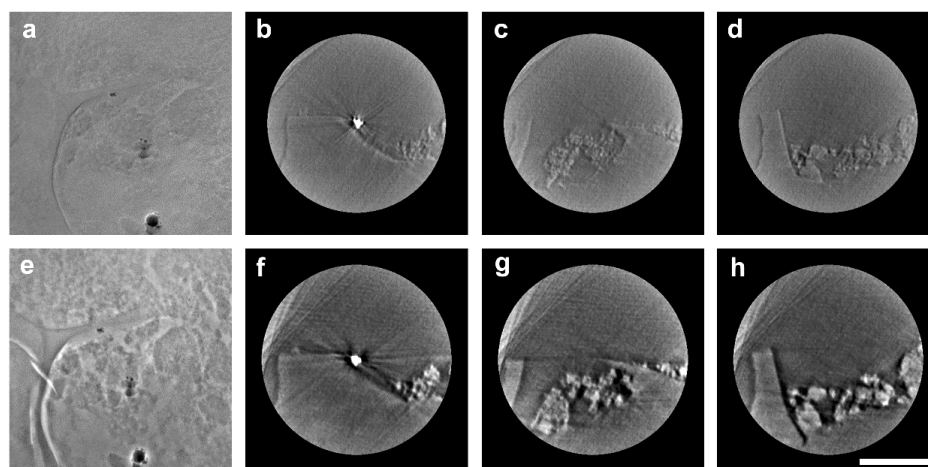


- 1 Özçimen, D. and Ersoy-Meriçboyu, A.: Characterization of biochar and bio-oil samples
2 obtained from carbonization of various biomass materials, *Renew. Energy*, 35,
3 1319-1324, 2010.
- 4 Rasmussen, C., Torn, M. S., and Southard, R. J.: Mineral assemblage and aggregates
5 control carbon dynamics in a California conifer forest, *Soil Sci. Soc. Am. J.*, 69,
6 1711-1721, 2005.
- 7 Rawal, A., Joseph, S. D., Hook, J. M., Chia, C. H., Munroe, P. R., Donne, S., Lin, Y.,
8 Phelan, D., Mitchell, D. R. G., Pace, B., Horvat, J., and Webber, J. B. W.: Mineral-
9 Biochar Composites: Molecular Structure and Porosity, *Environ. Sci. Technol.*, 50,
10 7706-7714, 2016.
- 11 Schmidt, M. W. I.: Biogeochemistry: Carbon budget in the black, *Nature*, 427, 305-307,
12 2004.
- 13 Sharma, R. K., Wooten, J. B., Baliga, V. L., Lin, X., Geoffrey Chan, W., and Hajaligol,
14 M. R.: Characterization of chars from pyrolysis of lignin, *Fuel*, 83, 1469-1482, 2004.
- 15 Sollins, P., Kramer, M. G., Swanston, C., Lajtha, K., Filley, T., Aufdenkampe, A. K.,
16 Wagai, R., and Bowden, R. D.: Sequential density fractionation across soils of
17 contrasting mineralogy: evidence for both microbial- and mineral-controlled soil
18 organic matter stabilization, *Biogeochemistry*, 96, 209-231, 2009.
- 19 Solomon, D., Lehmann, J., Harden, J., Wang, J., Kinyangi, J., Heymann, K.,
20 Karunakaran, C., Lu, Y., Wirick, S., and Jacobsen, C.: Micro- and nano-
21 environments of carbon sequestration: Multi-element STXM-NEXAFS
22 spectromicroscopy assessment of microbial carbon and mineral associations,
23 *Chem. Geol.*, 329, 53-73, 2012.
- 24 Sposito, G.: *The Chemistry of Soils*, Oxford University Press, 1989.
- 25 Torn, M. S., Trumbore, S. E., Chadwick, O. A., Vitousek, P. M., and Hendricks, D. M.:
26 Mineral control of soil organic carbon storage and turnover, *Nature*, 389, 170-173,
27 1997.
- 28 Vogel, C., Mueller, C. W., Hoschen, C., Buegger, F., Heister, K., Schulz, S., Schloter,
29 M., and Kogel-Knabner, I.: Submicron structures provide preferential spots for
30 carbon and nitrogen sequestration in soils, *Nat. Commun.*, 5, 2947, 2014.



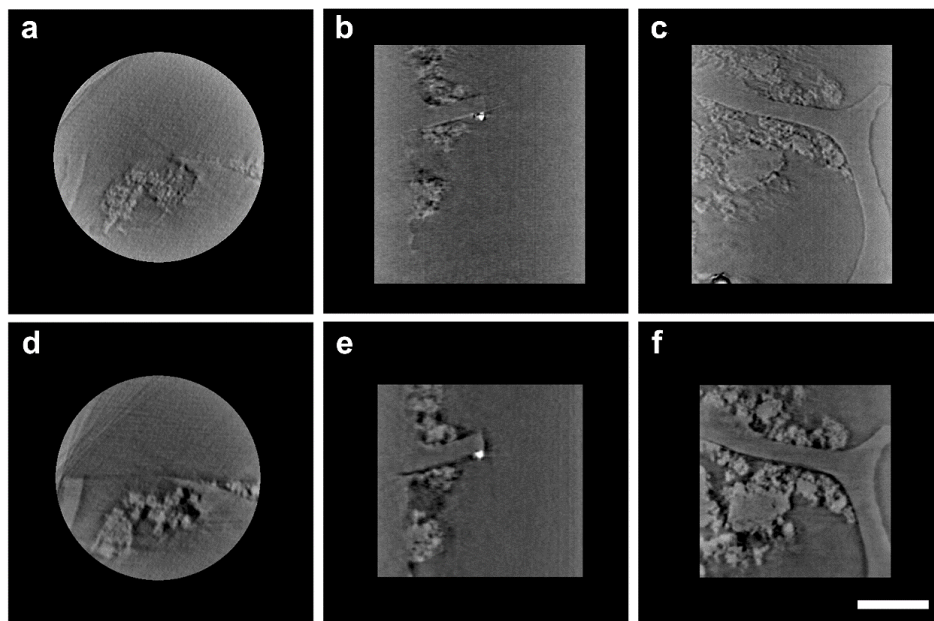
- 1 Wang, C.-C., Song, Y.-F., Song, S.-R., Ji, Q., Chiang, C.-C., Meng, Q., Li, H., Hsiao, K.,
2 Lu, Y.-C., Shew, B.-Y., Huang, T., and Reisz, R. R.: Evolution and Function of
3 Dinosaur Teeth at Ultramicrostructural Level Revealed Using Synchrotron
4 Transmission X-ray Microscopy, *Sci. Rep.*, 5, 15202, 2015.
- 5 Zbik, M. S., Frost, R. L., Song, Y. F., Chen, Y. M., and Chen, J. H.: Transmission X-ray
6 microscopy reveals the clay aggregate discrete structure in aqueous environment,
7 *J. Colloid Interf. Sci.*, 319, 457-461, 2008.
- 8 Zhao, Q., Poulson, S. R., Obrist, D., Sumaila, S., Dynes, J. J., McBeth, J. M., and Yang,
9 Y.: Iron-bound organic carbon in forest soils: quantification and characterization,
10 *Biogeosciences*, 13, 4777-4788, 2016.

11
12
13
14
15
16



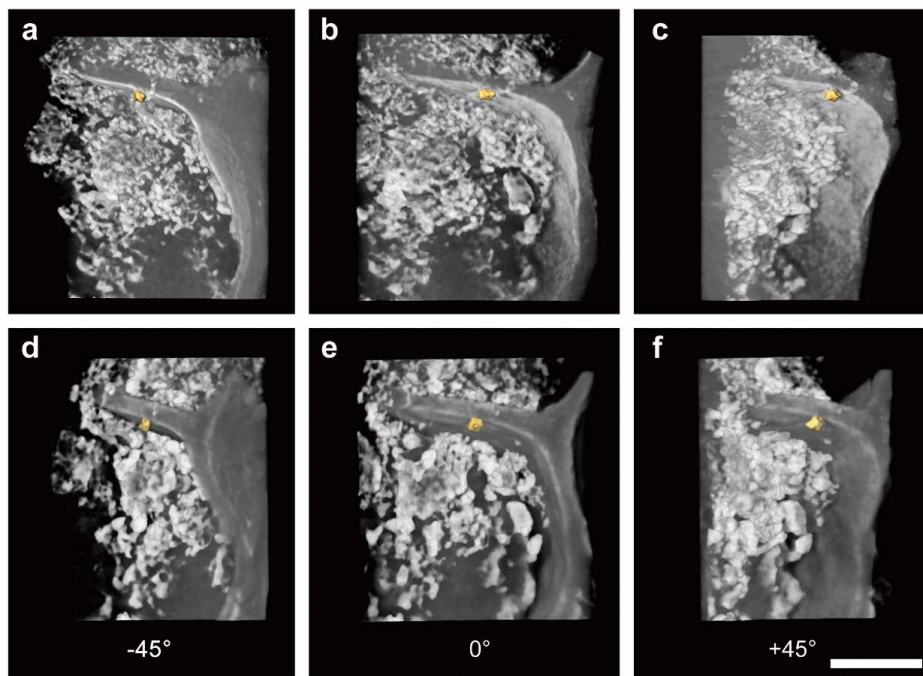
17
18
19
20

Figure 1.



1
2
3
4

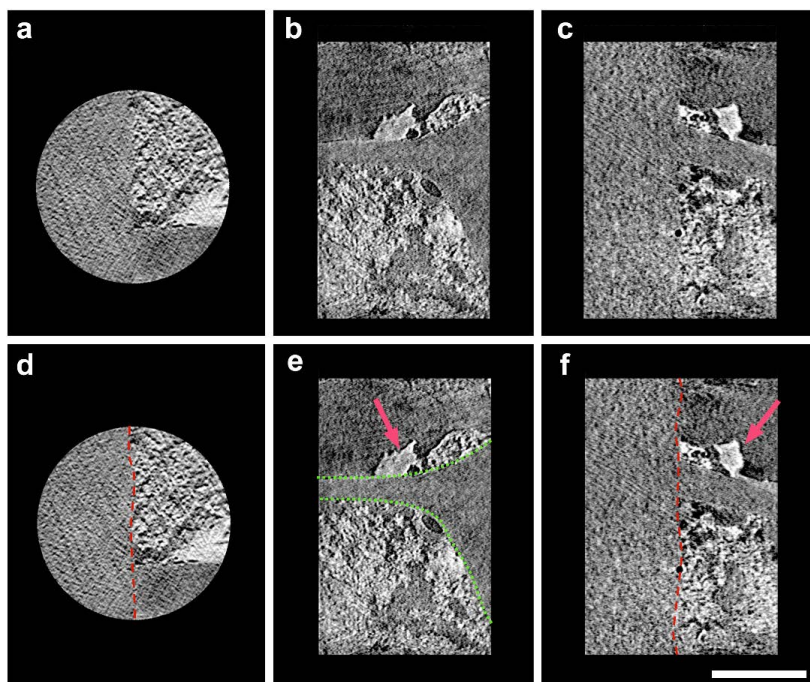
Figure 2.



1

2 **Figure 3.**

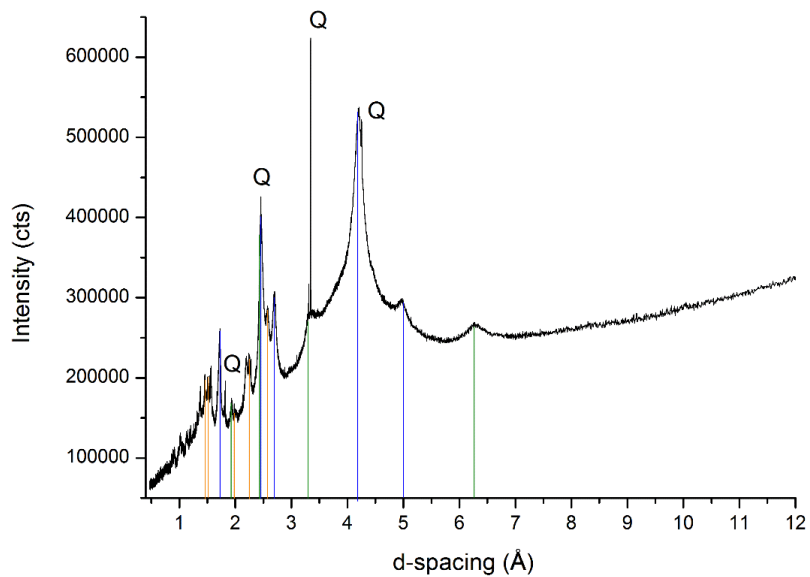
3



1

2

3 **Figure 4.**

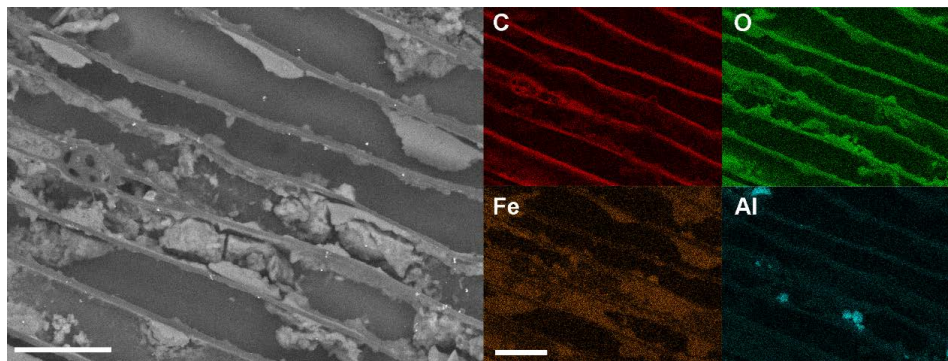


1

2 **Figure 5.**

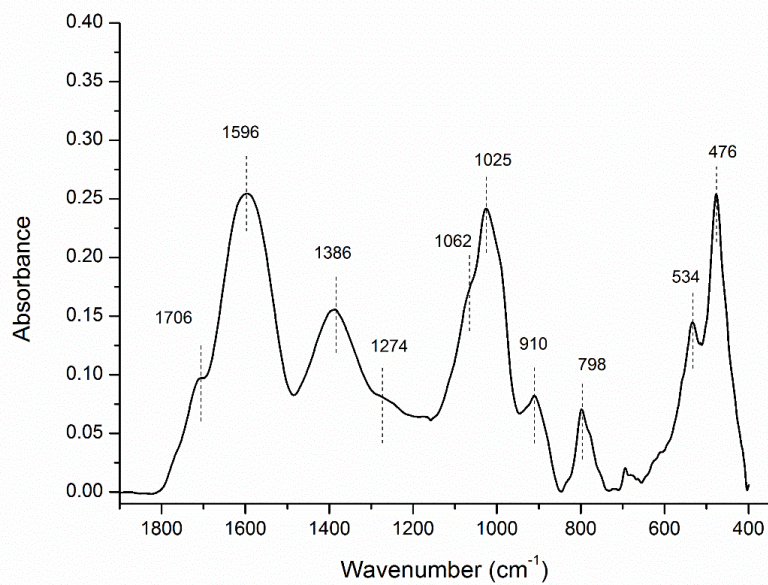
3

4



5

6 **Figure 6.**



1

2 **Figure 7.**

3